Acta Cryst. (1999). A**55**, 413–422

Theory of moiré fringes on X-ray diffraction topographs of bicrystals

Michael Ohler[a,b] and Jürgen Härtwig[b]*

[a]*Arbeitsgruppe Röntgenbeugung, Institut für Physik, Humboldt-Universität Berlin, Hausvogteiplatz 5-7, D-10117 Berlin, Germany, and* [b]*European Synchrotron Radiation Facility, BP 220, F-38043 Grenoble, France. E-mail: haertwig@esrf.fr*

(*Received 31 March 1998; accepted 3 August 1998*)

Abstract

The theory of moiré fringes on X-ray diffraction topographs of bicrystals is derived from the dynamical theory of X-ray diffraction for the reflection (Bragg) and the transmission (Laue) case. The influence on the moiré fringes of the diffraction geometry, of the geometry of the sample, of its optical properties and of the topographic method is investigated. The perfect-crystal theory is also expanded to weakly deformed bicrystals.

1. Introduction

Diffraction moiré fringes can be observed on X-ray or electron diffraction topographs of bicrystals. The first experimental evidence of such fringes was obtained by Mitsuishi *et al.* (1951) using transmission electron microscopy. Analysis of moiré fringes can, for example, serve in the study of dislocations (Bassett *et al.*, 1958). X-ray diffraction moiré fringes can be observed on topographs of *LLL* interferometers (Bonse & Hart, 1965; Gerward, 1978; Aboyan & Arshakyan, 1993) and of bicrystals (Chikawa, 1965; Lang, 1968; Jiang *et al.*, 1990). X-ray moiré topography is able to reveal lattice-parameter differences and rotations between crystal plates in the range from 10^{-4} to 10^{-9}, which leads to numerous applications (Hart, 1975).

The theory of diffraction moiré fringes was first developed for the case of electron diffraction (Hashimoto *et al.*, 1961; Gevers, 1962). A translation of the final results to the case of X-rays is found in the work of Chikawa (1967). Simon & Authier (1968) derived a theory of moiré fringes from Takagi's equations. Kato (1974) presented a theory for both spherical and plane waves of the X-ray diffraction by a bicrystal containing a misfit boundary. A detailed investigation of the same general situation and of many special cases was undertaken by Polcarová (1978, 1980). Recently, the theory of the moiré effect was reconsidered by Yoshimura (1996) in the frame of a 'non-projectivity' observed on a series of moiré topographs. The properties of the so-called 'translation-fault fringes' were described by Bonse & Hart (1968) and experimentally investigated by Bonse *et al.* (1969). Later, Ohler *et al.* (1997) showed that translation-fault fringes are nothing but moiré fringes.

Despite the large number of publications on diffraction moiré fringes, their description is still not complete. For example, no theoretical and almost no experimental study of the moiré effect in the Bragg case has been published. Moreover, important properties of the moiré fringes have not yet been clearly derived from the theory of X-ray diffraction. The aim of the present article is to give a compact formulation that allows one to understand in a convenient way the properties of moiré fringes, their dependence on the diffraction geometry (transmission or reflection, asymmetry, non-coplanarity), on the sample geometry (gap and crystal thicknesses), on the optical properties (absorption, refractive index) and on the topographic method (plane-monochromatic or integrated-wave topographs). The present work also puts together several aspects of the moiré effect that have already been described in the literature and it forms the basis for quantitative studies of moiré fringes on X-ray topographs (Ohler *et al.*, 1996, 1999; Prieur *et al.*, 1996).

2. Dynamical X-ray diffraction for the case of a bicrystal

This article is restricted to bicrystals with plane parallel surfaces and interfaces, which is the most common situation for bicrystals produced by ion implantation. However, small deviations will be considered and a generalization for interfaces with any orientation is possible. We use the level of approximation of the classical dynamical theory which is a quadratic approximation for the dispersion equation. Hence, diffraction geometries with grazing beam incidence or beam exit or Bragg angles close to 90° must be excluded (but in principle the approach presented in this paper may be further developed to be applied to such cases). Then, Abele's matrix formalism of the dynamical theory of X-ray scattering (Berreman, 1976) greatly simplifies the calculation and also allows the present formulation to be expanded to samples composed of more than two crystal plates. In Appendix *A*, the matrix is derived that relates the amplitudes $e_{0,e}$ and $e_{H,e}$ at the entrance surface to the amplitudes $e_{0,a}$ and $e_{H,a}$ at the exit surface of a single-crystal plate:

ISSN 0108-7673

$$\begin{pmatrix} e_{0,a} \\ e_{H,a} \end{pmatrix} = \mathbf{A}\begin{pmatrix} e_{0,e} \\ e_{H,e} \end{pmatrix}, \quad \mathbf{A} = \Psi\begin{pmatrix} \tau_0\varphi_{00} & \rho_0\varphi_{H0} \\ \rho_H\varphi_{0H} & \tau_H\varphi_{HH} \end{pmatrix}. \tag{1}$$

The transmission coefficients along the forward-diffracted and diffracted directions, τ_0 and τ_H, respectively, the reflection coefficients in these two directions, ρ_0 and ρ_H, respectively, and the phase factors $\varphi_{GG'}$ (from here on G and G' are both either 0 or H) and Ψ are given in Appendix A in such a way that equation (1) is valid for the Laue case (where $e_{H,e} = 0$) and the Bragg case (where $e_{H,a} = 0$).

It is convenient to use this matrix formulation to describe the diffraction by a bicrystal. Fig. 1 then shows that for the Laue case the diffraction by the second crystal can be described by two matrices, the matrix $\mathbf{B}_0$, related to the forward-diffracted beam from the first crystal, and the matrix $\mathbf{B}_H$, related to the diffracted beam from the first crystal. In the Bragg case, the infinite number of diffraction events by both crystals can be accounted for with an infinite number of diffraction matrices, $\mathbf{A}^{(n)}$ and $\mathbf{B}^{(n)}$ from the first and second crystals, respectively.

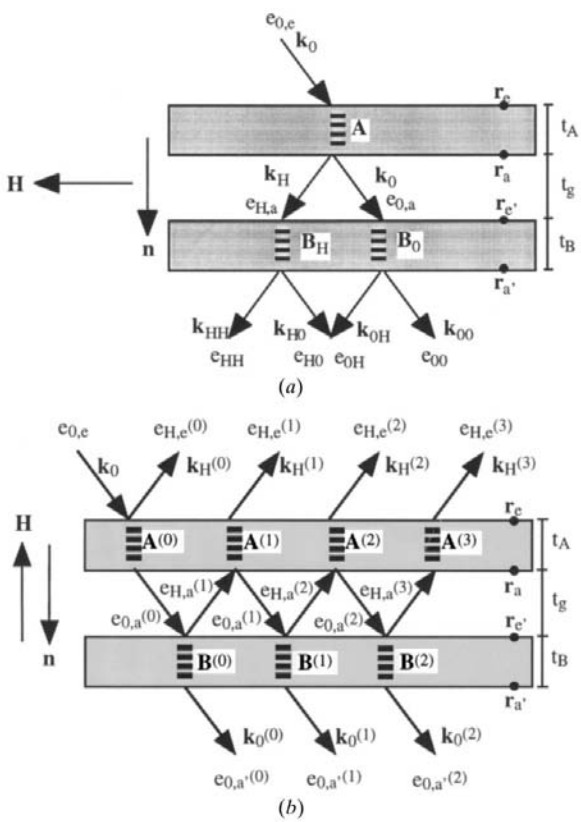

Fig. 1. The wave vectors, diffraction vectors, amplitudes, surfaces, interfaces and the matrices that characterize the diffraction process for (*a*) the Laue and (*b*) the Bragg case.

2.1. *Laue case*

For the Laue case, $\mathbf{B}_0$ and $\mathbf{B}_H$ can be put together to give a single matrix $\mathbf{B}$. The first column in the matrix $\mathbf{B}$ of the equation comes from $\mathbf{B}_0$ and describes the diffraction by the second crystal of the forward-diffracted wave from the first crystal. The second column in $\mathbf{B}$ comes from $\mathbf{B}_H$ and describes the diffraction by the second crystal of the diffracted wave from the first crystal. In the matrix $\mathbf{B}$, the transition through the gap and the phase accumulated behind the second crystal can be included:

$$\mathbf{B} = \begin{bmatrix} \Gamma_0\Psi_0\tau_{00}\varphi_{00,B}\exp(2\pi i\mathbf{k}_{00}\cdot\mathbf{r}) & \Gamma_H\Psi_H\rho_{H0}\varphi_{H0,B}\exp(2\pi i\mathbf{k}_{H0}\cdot\mathbf{r}) \\ \Gamma_0\Psi_0\rho_{0H}\varphi_{0H,B}\exp(2\pi i\mathbf{k}_{0H}\cdot\mathbf{r}) & \Gamma_H\Psi_H\tau_{HH}\varphi_{HH,B}\exp(2\pi i\mathbf{k}_{HH}\cdot\mathbf{r}) \end{bmatrix}. \tag{2}$$

The transmission and reflection coefficients, τ_{GG} and $\rho_{G,G'\neq G}$, the phase factors, $\varphi_{GG',B}$ and Ψ_G, the coefficients for the transition through the gap, Γ_G, and the wave vectors, $\mathbf{k}_{GG'}$, can be found in Appendix B; $\mathbf{r}$ is an arbitrary position behind the bicrystal.

Now, the amplitudes at any position on the exit surface of the bicrystal, $\mathbf{r}_S = \mathbf{r}_{a'} + \mathbf{x}$ (with $\mathbf{x}$ parallel to the sample surface), can be calculated from the amplitudes at the entrance surface, $e_{0,e}$ and $e_{H,e} = 0$, by multiplying the matrices in (1) and (2). The forward-diffracted and diffracted intensities are then:

$$I_0(\mathbf{r}_S) = |e_{0,e}\Gamma_0\Psi\Psi_0|^2\left\{|\tau_0\tau_{00}|^2 + \left|\frac{\Gamma_H\Psi_H}{\Gamma_0\Psi_0}\rho_H\rho_{H0}\right|^2 + 2\mathrm{Re}[\tau_0\tau_{00}\rho_H^*\rho_{H0}^*\exp(2\pi i\Phi_{\mathrm{Laue}})]\right\}$$

$$I_H(\mathbf{r}_S) = |e_{0,e}\Gamma_0\Psi\Psi_0|^2\left\{|\tau_0\rho_{0H}|^2 + \left|\frac{\Gamma_H\Psi_H}{\Gamma_0\Psi_0}\rho_H\tau_{HH}\right|^2 + 2\mathrm{Re}[\tau_0\tau_{HH}^*\rho_H^*\rho_{0H}\exp(2\pi i\Phi_{\mathrm{Laue}})]\right\}. \tag{3a}$$

Here, an asterisk (*) indicates the complex conjugate and Re the real part. The phase Φ_{Laue} can be decomposed into one contribution that varies spatially, the moiré effect, and others that are spatially constant and are due to the gap thickness t_g, the difference of the refractive indices between the gap and the crystal $\Delta\chi = \chi_0 - \chi_{0,g}$ and the reciprocal-lattice vector difference $\Delta\mathbf{H}$:

$$\Phi_{\mathrm{Laue}} = \Phi_{\mathrm{moiré}} + \Phi_{\mathrm{gap}} + \Phi_{\mathrm{refr}} + \Phi_{\Delta\mathbf{H},\mathrm{Laue}} \tag{3b}$$

with

$$\Phi_{\mathrm{moiré}} = \Delta\mathbf{H}\cdot\mathbf{r}_S, \quad \Phi_{\mathrm{gap}} = -\eta\frac{t_g}{\Lambda_0}, \quad \Phi_{\mathrm{refr}} = \frac{\Delta\chi}{2}\Delta\gamma k t_g,$$

$$\Phi_{\Delta\mathbf{H},\mathrm{Laue}} = -t_b\frac{\Delta\mathbf{H}}{2}\cdot\left(\frac{\mathbf{s}_H}{\gamma_H} + \frac{\mathbf{s}_0}{\gamma_0}\right).$$

[For the definitions of the symbols used in (3*b*) see Appendices *A* and *B*.]

The expressions (3*a*) and (3*b*) contain many special cases that are discussed in detail in the literature. For example, when $t_g = 0$ and $\Delta\mathbf{H} = 0$, they lead to the diffracted and transmitted intensities of a perfect single-crystal plate with the thickness of the bicrystal. For $t_g = 0$ and $\Delta\mathbf{H} \neq 0$, one obtains the solutions given by Polcarová (1978, 1980) for plane parallel interfaces. Moreover, when $t_g \neq 0$ and $\Delta\mathbf{H} = 0$, intensity modulations on the rocking curve are expected when t_g reaches the scale of the *Pendellösung* length Λ_0 (Yoshimura, 1991). For a large $\Delta\mathbf{H}$, the distance between the moiré fringes is small and only the first two terms of $I_0(\mathbf{r}_S)$ and $I_H(\mathbf{r}_S)$ in equation (3*a*) contribute to the measured intensity because the terms Re[...] are cancelled out (Gaca, 1974).

2.2. *Bragg case*

The Bragg case has been studied intensively in the frame of X-ray diffractometry. This technique averages over the lateral extension of the sample. However, for the moiré topography, the locally diffracted intensity must be determined. For practical reasons, only the diffracted waves are considered here, but the expressions for the waves transmitted through the sample can be derived in a similar way. Following Appendix *C*, one is able to obtain the coefficients of the diffraction matrices $\mathbf{A}^{(n)}$ and $\mathbf{B}^{(n)}$, where $\mathbf{B}^{(n)}$ includes the transmission through the gap:

$$\mathbf{A}^{(n)} = \Psi_A^{(n)} \begin{bmatrix} \tau_{0A}^{(n)}\varphi_{00,A}^{(n)} & \rho_{0A}^{(n)}\varphi_{H0,A}^{(n)} \\ \rho_{HA}^{(n)}\varphi_{0H,A}^{(n)} & \tau_{HA}^{(n)}\varphi_{HH,A}^{(n)} \end{bmatrix}$$
$$\mathbf{B}^{(n)} = \Psi_B^{(n)} \begin{bmatrix} \Gamma_0\tau_{0B}^{(n)}\varphi_{00,B}^{(n)} & \Gamma_H\rho_{0B}^{(n)}\varphi_{H0,B}^{(n)} \\ \Gamma_0\rho_{HB}^{(n)}\varphi_{0H,B}^{(n)} & \Gamma_H\tau_{HB}^{(n)}\varphi_{HH,B}^{(n)} \end{bmatrix}. \quad (4)$$

From Fig. 1, one now reads matrix equations that allow one to find a recursion formula for the diffracted amplitudes $e_{H,e}^{(n)}$. The total diffracted intensity at any position in the entrance surface, $\mathbf{r}_S = \mathbf{r}_e + \mathbf{x}$, is then $I_H^{\text{tot}}(\mathbf{r}_S) = |\sum e_{H,e}^{(n)} \exp[2\pi i \mathbf{k}_H^{(n)} \cdot \mathbf{r}_S]|^2$. With Appendix *C* one finds:

$$I_H^{\text{tot}}(\mathbf{r}_S) = |e_{0,e}^{(0)}|^2 \left| \frac{\rho_{HA}^{(0)}}{\tau_{HA}^{(0)}} + \frac{\rho_{HB}^{(0)}}{\tau_{HA}^{(0)}\tau_{HA}^{(1)}\tau_{HB}^{(0)}} \times \left\{ \exp[2\pi i \Phi_{\text{Bragg}}^{(1)}] - \sum_{n=2}^{\infty} (-1)^n \exp[2\pi i \Phi_{\text{Bragg}}^{(n)}] \times \prod_{j=2}^{n} \left[\frac{\rho_{0A}^{(j-1)}\rho_{HB}^{(j-1)}}{\tau_{HA}^{(j)}\tau_{HB}^{(j-1)}} \right] \right\} \right|^2 \quad (5a)$$

$$\Phi_{\text{Bragg}}^{(n)} = n(\Phi_{\text{moiré}} + \Phi_{\text{gap}} + \Phi_{\text{refr}} + \Phi_{\Delta\mathbf{H},\text{Bragg}}) \quad (5b)$$

with

$$\Phi_{\text{moiré}} = \Delta\mathbf{H} \cdot \mathbf{r}_S, \quad \Phi_{\text{gap}} = -\eta \frac{t_g}{\Lambda_0}, \quad \Phi_{\text{refr}} = \frac{\Delta\chi}{2} \Delta\gamma k t_g,$$
$$\Phi_{\Delta\mathbf{H},\text{Bragg}} = (t_A + t_g) \frac{\Delta\mathbf{H}}{2} \cdot \left(\frac{\mathbf{s}_H}{\gamma_H} + \frac{\mathbf{s}_0}{\gamma_0} \right) + n t_g \frac{\Delta\mathbf{H}}{2} \cdot \left(\frac{\mathbf{s}_H}{\gamma_H} - \frac{\mathbf{s}_0}{\gamma_0} \right).$$

In equation (5*b*), the individual terms are similar to those for the Laue case (3*b*), only $\Phi_{\Delta\mathbf{H},\text{Bragg}}$ has one contribution from the first crystal (t_A) and another from the gap, whereas $\Phi_{\Delta\mathbf{H},\text{Laue}}$ has one contribution from the second crystal (t_B).

The equations (5*a*) and (5*b*) can also be discussed for several special cases. When $\Delta\mathbf{H}$ is parallel to the surface normal and for a $\Delta\mathbf{H}$ perpendicular to the diffraction plane, the sum in (5*a*) can be evaluated analytically (see Appendix *C*). This solution can also be used as an approximation for the intensity profile in some other cases. For $\Delta\mathbf{H} = 0$, as in the Laue case, the rocking curve shows intensity modulations when the gap thickness reaches the scale of the *Pendellösung* length. For a large $\Delta\mathbf{H}$ and for the first crystal in Bragg reflection, the second crystal is out of the reflection condition and thus only the first term in the sum of equation (5*a*) contributes to the diffracted intensity.

3. Properties of moiré fringes

3.1. *Geometrical properties*

For both the Bragg and the Laue case, the diffracted intensity is modulated with a periodicity given by the reciprocal-lattice vector difference $\Delta\mathbf{H}$, but only for the Laue case is it modulated with $\cos(\Delta\mathbf{H} \cdot \mathbf{r}_S)$. In the Bragg case, it has a contribution from the fundamental spatial frequency, $\Delta\mathbf{H}$, and from higher harmonics, $n\Delta\mathbf{H}$. In our experiments, the moiré patterns were always very similar to a cosine modulation for the Laue case, but very different from a cosine modulation for the Bragg case.

Moreover, the moiré fringes are projective for both the Bragg and the Laue case, which means that the moiré pattern is the diffracted intensity at the surface of the crystal projected on the film plane. This is a direct consequence of the elastic scattering process (all wave vectors outside the crystal have the same length) and the fact that no propagation (properties of the waves before and especially after the crystal) is included. Thus, the present theory cannot explain the 'non-projectiveness' observed by Yoshimura (1996).

The terms $\Phi_{\text{moiré}}$ in (3*b*) and (5*b*) also show that for perfect bicrystals the fringes are given by the component of $\Delta\mathbf{H}$ that is parallel to the sample surface, $\Delta\mathbf{H}_{\|}$: the moiré fringes are perpendicular to $\Delta\mathbf{H}_{\|}$ and have a spacing of $|\Delta\mathbf{H}_{\|}|^{-1}$. The component perpendicular to the

sample surface, $\Delta\mathbf{H}_\perp$, cannot be determined from the direction and the spacing of the moiré fringes because $\Delta\mathbf{H}_\perp$ is not related to a break of the translational symmetry of the sample (Ohler *et al.*, 1996). This holds for the Bragg and the Laue case. It is also independent from the asymmetry, the noncoplanarity (the incidence plane, parallel to the incident wave vector and the surface normal, and the diffraction plane, parallel to the incident wave vector and the diffraction vector, are not parallel) and the Bragg angle of the reflection. This result is important for the analysis of white-beam experiments in which many topographs are recorded in a single exposure but each with its own asymmetry, noncoplanarity and Bragg angle.

3.2. *Optical properties*

The influence on the moiré fringes of the difference between the refractive indices in the two crystals and the gap thickness is described by the terms $\Phi_{\rm refr}$ in (3*b*) and (5*b*). These terms can lead to a global displacement of the moiré pattern on the topograph; they only vanish for the symmetrical Laue case but they do not lead to a modification of the fringe direction or the interfringe spacing.

When high X-ray energies are used, the absorption in the sample may become very weak. When in addition the fringe spacing is much larger than the *Pendellösung* length, a contrast inversion is expected between the topographs recorded with the forward-diffracted and the diffracted beams (Appendix *B*). This is also expected for reasons of energy conservation.

Another case of great practical importance is an anomalous transmission (*e.g.* Batterman & Cole, 1964) through the thick part of a bicrystal and a negligible absorption in its thin part. Under such conditions, a contrast inversion is only expected when the thick plate is at the entrance side of the bicrystal. When the thick crystal is at the exit side, the moiré patterns recorded with the forward-diffracted and the diffracted beams have their maxima at the same position. This is demonstrated in Appendix *B*; a physical argument for the effect has been presented by Bonse & Hart (1968).

Such a contrast inversion has been attributed, however, to 'translation fault fringes' by Bonse & Hart (1968) and Bonse *et al.* (1969), but here, as in a previous work (Ohler *et al.*, 1997), it is seen that such 'translation fault fringes' are nothing but moiré fringes.

3.3. *Dependency of the position of the moiré pattern on the angular deviation from the kinematical Bragg condition*

Equations (3) show that for the Laue case the moiré pattern is given by a sine and a cosine term with amplitudes that depend on the deviation from the kinematical Bragg condition [see equation (18)], as does the absolute position of the moiré pattern.

It is shown in Appendix *D* that, for highly collimated and highly monochromatic radiation, the moiré pattern is translated over distances of one interfringe distance when the angular deviation from the kinematical Bragg condition, $\Delta\Theta$, varies by $\Delta\Theta/\omega_0 = 2\Lambda_0/(t_A + t_B)$ where ω_0 is the half-width (full width at half-maximum, or Prince–Darwin width) of the reflection.

In Appendix *D*, experiments with medium collimation and monochromaticity are investigated. Under such conditions, no displacement of the moiré fringes with a variation of $\Delta\Theta$ is expected when both crystal plates are much thicker than the *Pendellösung* length. When either of the two plates has a thickness t, which is much smaller than this length, such a dependence is very weak: a variation of $\Delta\Theta$ only results in a displacement of a fraction $\Delta\Theta t/(2\omega_0\Lambda_0)$ of a moiré fringe spacing.

3.4. *Fringe contrast on integrated wave topographs*

Often moiré fringes are recorded on 'integrated wave topographs' (Tanner, 1996), that means either with a white but highly collimated ('white-beam topography') or a quasi-monochromatic X-ray beam from a source with a large angular source size ('Lang topography'). This situation is investigated in Appendix *D* for the case of no absorption, a negligible gap thickness and a large distance between the moiré fringes. In Appendix *D*, the contrast of moiré fringes is studied as a function of the *Pendellösung* length for different thicknesses of the two crystals. For two crystals that are much thicker than the *Pendellösung* length, the contrast is 1/5 when the thicknesses of the two crystals are about the same. However, the contrast is 1/3 for two crystal plates that have very different thicknesses. When either of the crystals has a thickness comparable to or smaller than the *Pendellösung* length, the moiré contrast must be calculated numerically. Two examples are shown in Fig. 2.

4. Expansion to locally perfect bicrystals

In many practical cases, the reciprocal-lattice vector difference $\Delta\mathbf{H}$ depends on spatial coordinates and the bicrystal under study cannot be considered as perfect. When the effective misorientation (see Appendix *B*) is approximately constant over the 'effective area of the crystal' (Kuběna & Holý, 1983), the theory of the perfect crystal can be expanded for a deformed crystal on a local scale (Härtwig *et al.*, 1988). The same is possible for a deformed bicrystal but then the phase shift due to the moiré effect, $\Phi_{\rm moiré}$ in equations (3*b*) and (5*b*), must be calculated in a cumulative manner between an arbitrary reference point $\mathbf{r}_0$ and the observation point $\mathbf{r}_S$:

$$\Phi_{\text{moiré}}(\mathbf{r}_S) = \int_{\mathbf{r}_0}^{\mathbf{r}_S} \Delta\mathbf{H}(\mathbf{r}')\,\mathrm{d}\mathbf{r}'$$
$$= -\int_{\mathbf{r}_0}^{\mathbf{r}_S} \mathrm{grad}[\mathbf{H}\cdot\mathbf{u}(\mathbf{r}')]\,\mathrm{d}\mathbf{r}'$$
$$= -\mathbf{H}\cdot\mathbf{u}(\mathbf{r}_S) + \text{constant}.$$

Here, $\mathbf{u}(\mathbf{r})$ is the displacement field of the atomic positions in one crystal relative to the atomic positions in the other. For a perfect bicrystal, $\mathbf{u}(\mathbf{r})$ is a linear function in $\mathbf{r}$ and in this case $\Delta\mathbf{H}\cdot\mathbf{r}$ and $-\mathbf{H}\cdot\mathbf{u}(\mathbf{r})$ are equivalent. For deformed bicrystals, the diffracted intensity also depends on the local effective misorientation. Close to crystal defects, both contributions to the contrast must be considered but can be separated experimentally (Prieur *et al.*, 1996). Far from defects, the spatial variations of the diffracted intensity mainly depend on $\Phi_{\text{moiré}} = -\mathbf{H}\cdot\mathbf{u}(\mathbf{r})$ and a new moiré fringe is introduced in the pattern each time this function equals an integer. This allows the three components of the displacement field $\mathbf{u}(\mathbf{r})$ to be reconstructed from moiré topographs, with an interferometric resolution (Ohler *et al.*, 1999).

When the thicknesses of the crystal or the gap vary, the surface and interface normals are not parallel. It may be shown that such non-homogeneities enter in the expressions for the diffracted intensity as factors of small quantities [like the *Anpassung* $\delta^{(j)}$, see Appendix *A*]. Hence, small spatial variations of the interface orientations lead to second-order contributions and can be neglected. This means that the equations (3) and (6) are valid on a local scale when crystal and gap thicknesses vary slowly over the sample. Then, variations of the gap thickness only influence the moiré fringes when they reach the scale of the *Pendellösung* length [Φ_{gap} in equations (3*b*) and (5*b*)]; the same holds for variations of the crystal thicknesses [τ_{G}, ρ_{G} in equation (10)].

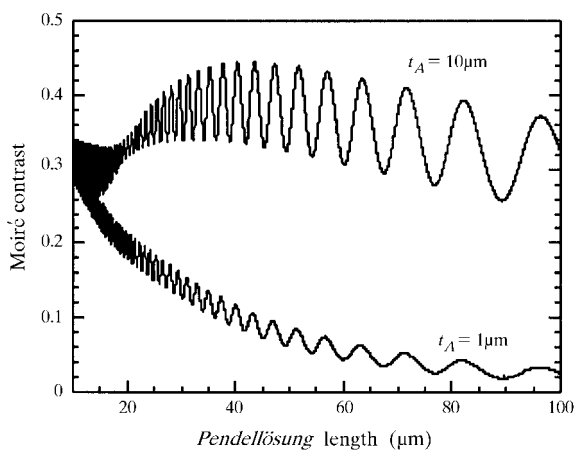

Fig. 2. The moiré contrast on integrated wave topographs in the Laue case for different *Pendellösung* distances. Two different thicknesses of the first crystal plate for a thickness of 550 μm for the second crystal plate. The contrast oscillations are mainly due to the oscillations of the integrated intensity of the thick crystal plate.

Often heterostructures like bicrystals are bent. It has been shown by Ohler *et al.* (1996) that the influence of the sample bending on the moiré fringes scales with the gap thickness and that for cubic crystals $\Delta H_i = h_i t_{\text{gap}}/(a_0 R_i)$ is a good estimation (h_i are the Miller indices of the reflection, R_i the bending radii, ΔH_i the components of the additional reciprocal-lattice vector difference, and a_0 is the lattice parameter). The sign of the bending radius can be inverted by interchanging the beam entrance surface and the beam exit surface. Hence, with a comparison of two such moiré topographs, the influence of the bending and of the reciprocal-lattice vector difference can be separated.

5. Summary

In the Laue and in the Bragg case the main source of contrast variations on X-ray moiré topographs of locally perfect bicrystals is the function $\mathbf{H}\cdot\mathbf{u}(\mathbf{r}_S)$ where $\mathbf{H}$ is the diffraction vector and $\mathbf{u}(\mathbf{r})$ is the displacement field between the atomic positions in one crystal referred to the atomic positions in the other. Here, $\mathbf{r}_S$ is an observation point in the crystal surface. Spatial variations of crystal and gap thickness as well as the variations of the effective misorientation in weakly deformed bicrystals can be described by applying the perfect-crystal theory on a local scale. Only crystal and gap thickness variations that are of the order of the *Pendellösung* length or more may alter the moiré fringes. The intensity profile of the moiré pattern in the Laue case is different from that in the Bragg case, but the asymmetry and the non-coplanarity of the reflection have no influence on the fringe spacing and the fringe direction. For experiments with high collimation and monochromaticity, the position of the moiré pattern is very sensitive to the deviation from the kinematical Bragg condition. However, for the experimental conditions of medium collimation and monochromaticity, the situation is different: the position of the moiré pattern does not vary with the deviation from the kinematical Bragg condition when both crystal plates are much thicker than the *Pendellösung* length. The displacement of the fringes is very small when either of the two plates is much thinner than the *Pendellösung* length. Finally, the contrast of moiré fringes on integrated wave topographs can be calculated numerically.

APPENDIX *A*
Diffraction matrix for a single-crystal plate

The waves within a crystal are described by the 'fundamental equation of the dynamical theory' (*e.g.* Batterman & Cole, 1964):

$$\begin{bmatrix} 2k\xi_0^{(j)} & -k^2 P\chi_{\bar{H}} \\ -k^2 P\chi_H & 2k\xi_H^{(j)} \end{bmatrix} \begin{bmatrix} E_0^{(j)} \\ E_H^{(j)} \end{bmatrix} = 0. \qquad (6)$$

Here, k is the vacuum wave number and the $\xi_G^{(j)} = |\mathbf{K}_G^{(j)}| - k(1 + \chi_0/2)$ are the complex excitation errors [with $|\mathbf{a}| = (\mathbf{a} \cdot \mathbf{a})^{1/2}$], $\mathbf{K}_0^{(j)} = \mathbf{k}_0 - \delta^{(j)}\mathbf{n}$ and $\mathbf{K}_H^{(j)} = \mathbf{K}_0^{(j)} + \mathbf{H}$ are the wave vectors, and $E_0^{(j)}$ and $E_H^{(j)}$ the amplitudes inside the crystal for both sheets ($j = 1, 2$) of the dispersion surface. The $\delta^{(j)}$ are the *Anpassung* (Laue, 1960) along the surface normal $\mathbf{n}$ of the wave vectors inside the crystal to the incident vacuum wave vector $\mathbf{k}_0$. The polarization factor is $P = 1$ or $P = \cos 2\Theta$ (Θ is the Bragg angle) depending on the polarization state, and χ_0, χ_H and $\chi_{\bar{H}}$ are the Fourier components of the dielectric susceptibility. The wave vector of the diffracted wave outside the crystal is given by $\mathbf{k}_H = \mathbf{k}_0 + \mathbf{H} - g_H\mathbf{n}$, where $g_H = -\Delta\Theta k \sin(2\Theta)/\gamma_H$ with $\Delta\Theta$ for the angular deviation from the kinematical Bragg condition. Moreover, $\gamma_G = \mathbf{n} \cdot \mathbf{s}_G$, where $\mathbf{s}_G$ are the unit vectors in the forward-diffracted ($G = 0$) and diffracted ($G = H$) directions. It is then possible to derive a quadratic equation for the *Anpassung* $\delta^{(j)}$ from equation (6), which also provides the amplitude ratios $c^{(j)} = E_H^{(j)}/E_0^{(j)}$ in the crystal:

$$\begin{aligned} \delta^{(j)} &= -\tfrac{1}{2}[k\chi_0/\gamma_0 + (\eta \pm y)/\Lambda_0] \\ c^{(j)} &= -(P/|P|)(\gamma_0\chi_H/|\gamma_H|\chi_{\bar{H}})^{1/2}(\eta \pm y). \end{aligned} \tag{7}$$

Here, $\Lambda_0 = (\gamma_0|\gamma_H|/\chi_H\chi_{\bar{H}})^{1/2}/k|P|$ is the complex *Pendellösung* length, $y = (\eta^2 + \sigma)^{1/2}$, and $\sigma = 1$ for the Laue case and $\sigma = -1$ for the Bragg case. The $\pm$ signs refer to the two wave fields in the crystal related to the two tie points excited on the branches of the dispersion surface (Batterman & Cole, 1964). The normalized angular coordinate η (Batterman & Cole, 1964), also known as the 'deviation parameter' η^A (Authier, 1961, 1992), was probably first used by Zachariasen (1945) and is defined here in a general way as

$$\begin{aligned} \eta &= -\Lambda_0[(|\mathbf{k}_0 + \mathbf{H}| - k)/\gamma_H - \delta g] \\ &= -\Lambda_0(g_H - \delta g) = \sigma\eta^A, \end{aligned} \tag{8}$$

where $\delta g = k\Delta\gamma\chi_0/2$ with $\Delta\gamma = \gamma_H^{-1} - \gamma_0^{-1}$. The use of the parameter η instead of η^A has consequences with respect to the form of equation (8) concerning the appearance of a factor σ. The definition of η in (8) allows one to calculate, in a convenient way, the deviation parameter for any incident wave vector and any diffraction vector, and also for non-coplanar diffraction geometries as long as the quadratic approximation for the dispersion equation is justified. However, equation (8) must be interpreted correctly: when $\mathbf{k}_H$ is the incident wave vector and $-\mathbf{H}$ the diffraction vector, γ_H and γ_0 need to be interchanged and $\delta^{(j)}$ is the *Anpassung* to $\mathbf{k}_H$ and not to $\mathbf{k}_0$ which inverts the sign of η.

The amplitudes outside and inside the crystal are related by the boundary conditions:

$$\begin{aligned} e_{G,\nu}\exp(2\pi i\mathbf{k}_G \cdot \mathbf{r}_\nu) &= \sum_{j=1,2} E_G^{(j)} \exp[2\pi i\mathbf{K}_G^{(j)} \cdot \mathbf{r}_\nu] \\ \Rightarrow e_{G,\nu}\varphi_{G,\nu} &= \sum_{j=1,2} E_G^{(j)}\Phi_\nu^{(j)} \\ \varphi_{0,\nu} &= 1 \\ \varphi_{H,\nu} &= \exp[2\pi i(\mathbf{k}_H - \mathbf{k}_0 - \mathbf{H}) \cdot \mathbf{r}_\nu] \\ \Phi_\nu^{(j)} &= \exp[-2\pi i\delta^{(j)}\mathbf{n} \cdot \mathbf{r}_\nu]. \end{aligned} \tag{9}$$

In these equations, $G = 0$, H and ν is either 'e' or 'a' for the entrance or the exit surface, respectively. Together with the equations (7), the coefficients in the matrix $\mathbf{A}$ in equation (1) are:

$$\begin{aligned} \tau_0 &= \cos(A_A y) - (i\eta/y)\sin(A_A y) \\ \tau_H &= \cos(A_A y) + (i\eta/y)\sin(A_A y) \\ \rho_0 &= (iP/|P|)(\chi_{\bar{H}}|\gamma_H|/\chi_H\gamma_0)^{1/2}\sin(A_A y)/y \\ \rho_H &= (i\sigma P/|P|)(\chi_H\gamma_0/\chi_{\bar{H}}|\gamma_H|)^{1/2}\sin(A_A y)/y \\ \varphi_{00} &= 1 \\ \varphi_{0H} &= \exp[-2\pi i(\mathbf{k}_H - \mathbf{k}_0 - \mathbf{H}) \cdot \mathbf{r}_a] \\ \varphi_{H0} &= \exp[2\pi i(\mathbf{k}_H - \mathbf{k}_0 - \mathbf{H}) \cdot \mathbf{r}_e] \\ \varphi_{HH} &= \exp[-2\pi i(\mathbf{k}_H - \mathbf{k}_0 - \mathbf{H}) \cdot \mathbf{n}t_A] \\ \Psi &= \exp[\pi i t_A(k\chi_0/\gamma_0 + \eta/\Lambda_0)]. \end{aligned} \tag{10}$$

Here, $A_A = \pi t_A/\Lambda_0$ is the normalized crystal thickness of the first crystal. The equations (8), (9) and (10) are written in a way that the matrices for the second crystal in the Laue case and all matrices for both crystals in the Bragg case, for all diffraction orders, can be obtained from these equations by simple replacement rules. Furthermore, the relation $\tau_0\tau_H - \rho_0\rho_H = 1$ is valid for both the Bragg and the Laue case and is useful in many calculations.

APPENDIX *B*
Diffraction matrix of the second crystal plate in the Laue case

The wave vectors $\mathbf{k}_0$ and $\mathbf{k}_H$ from the first crystal are diffracted with the diffraction vectors $\mathbf{H} + \Delta\mathbf{H}$ and $-(\mathbf{H} + \Delta\mathbf{H})$ by the second crystal. The wave vectors behind the second crystal plate are then $\mathbf{k}_{00} = \mathbf{k}_0$, $\mathbf{k}_{0H} = \mathbf{k}_0 + \mathbf{H} + \Delta\mathbf{H} - (g_H + \Delta\mathbf{H} \cdot \mathbf{s}_H/\gamma_h)\mathbf{n}$ (both excited by $\mathbf{k}_0$) and $\mathbf{k}_{H0} = \mathbf{k}_0 - \Delta\mathbf{H} + (\Delta\mathbf{H} \cdot \mathbf{s}_0/\gamma_0)\mathbf{n}$, $\mathbf{k}_{HH} = \mathbf{k}_H$ (both excited by $\mathbf{k}_H$). The deviation parameters η_G in the second crystal, related to the wave vectors $\mathbf{k}_G$, are then found with equation (8) and the replacements $\mathbf{k}_0 \rightarrow \mathbf{k}_{G0}$ and $\mathbf{H} \rightarrow \mathbf{H} + \Delta\mathbf{H}$:

$$\begin{aligned} \eta_0 &= \eta - \Lambda_0(\Delta\mathbf{H} \cdot \mathbf{s}_H)/\gamma_H \\ \eta_H &= \eta - \Lambda_0(\Delta\mathbf{H} \cdot \mathbf{s}_0)/\gamma_0. \end{aligned} \tag{11}$$

The difference between η and the η_G corresponds to the effective misorientation (Authier, 1967), normalized to the width of the reflection curve. Using the η_G instead of

η in (8) provides the amplitude ratios and the *Anpassung* to $\mathbf{k}_{G0}$ of the wave vectors in the second crystal. The boundary conditions for the waves excited in the second crystal can now be obtained from (9) with the replacements: $\mathbf{k}_0 \rightarrow \mathbf{k}_{G0}$, $\mathbf{k}_H \rightarrow \mathbf{k}_{GH}$, $\mathbf{H} \rightarrow \mathbf{H} + \Delta\mathbf{H}$, $e \rightarrow e'$ and $a \rightarrow a'$. This also provides the phase factors $\varphi_{GG',B}$ in equation (2) from the $\varphi_{GG'}$ in equation (10). Finally, the τ_{00}, ρ_{0H} and Ψ_0 in (2) are obtained from τ_0, ρ_H and Ψ in (10) by replacing η by η_0, and the τ_{HH}, ρ_{H0} and Ψ_H by replacing η by η_H and by replacing t_A by t_B in all these functions. It is also possible to derive these results from geometrical constructions of the dispersion surfaces (Polcarová, 1978).

The relations between the transmission and reflection coefficients will now be discussed for two special cases: the case of negligible absorption and the case of anomalous absorption (Borrman effect). To simplify the discussion, the approximation $\eta_0 \simeq \eta_H$ will be made here. As can be seen from equation (11), this approximation is valid for a moiré fringe spacing much larger than the *Pendellösung* length. Nevertheless, the conclusions drawn here are also valid when $\eta_0 \neq \eta_H$.

For the case of no absorption, the arguments of the sine and cosine functions in equations (10) are real. It follows that for a non-absorbing second crystal $\rho_{0H} = -\rho^*_{H0}$ and $\tau_{00} = \tau^*_{HH}$. When the absorption is small, these equations still hold approximately: $\rho_{0H} \approx -\rho^*_{H0}$ and $\tau_{00} \approx \tau^*_{HH}$. For the case of an absorbing crystal plate, the imaginary parts of the arguments of the sine and cosine functions in equations (10) cannot be neglected. Using the relations $\cos z = [\exp(iz) + \exp(-iz)]/2$ and $\sin z = [\exp(iz) - \exp(-iz)]/2$, one can express the transmission and reflection coefficients by the contributions from the strongly and the weakly absorbed wavefields. In the case of anomalous transmission through the second crystal plate, the strongly absorbed wavefield can be neglected. Then, $\tau_{00} \approx \tau^*_{HH}$ still holds, but now $\rho_{0H} \approx +\rho^*_{H0}$. Details of such a calculation, not using the present formulation in terms of reflection and transmission coefficients, may, for example, be found in the work of Bonse & Hart (1968). These results can now be put into equations (3*a*): for a non-absorbing second crystal plate, the topographs recorded with the forward-diffracted and the diffracted beams display a contrast inversion, whereas the maxima and minima of the fringes are at the same locations on these two topographs for a second crystal plate in the anomalous absorption regime.

Finally, the phase factors due to the gap, Γ_G, in equation (2) can be found from the boundary conditions for the gap: $e_{G,\nu} \exp(2\pi i \mathbf{k}_G \cdot \mathbf{r}_\nu) = E_G \exp(2\pi i \mathbf{K}_G \cdot \mathbf{r}_\nu)$. Here $G = 0, H$, and ν is either a (exit surface of the first crystal) or e' (entrance surface of the second crystal) and $\mathbf{K}_G = \mathbf{k}_G + \mathbf{n}k\chi_{0,g}/(2\gamma_G)$ are the wave vectors in the gap. One obtains $e_{G,e'} = \Gamma_G e_{G,a}$, where $\Gamma_G = \exp[\pi i t_g (k\chi_{0,g}/\gamma_G)]$ with t_g and $\chi_{0,g}$ for the thickness and the dielectric susceptibility of the gap.

APPENDIX *C*
Diffraction matrices in the Bragg case

Contrary to the Laue case, in the Bragg case the waves scatter many times between the two crystals (see Fig. 1). This can be taken into account by labelling the wave vectors of the different scattering orders $\mathbf{k}_0^{(n)}$ and $\mathbf{k}_H^{(n)}$ for the forward-diffracted and the diffracted directions, respectively. As also seen in Fig. 1, the wave vector $\mathbf{k}_H^{(0)}$ is excited with a single diffraction from the first crystal (diffraction vector $\mathbf{H}$). All other $\mathbf{k}_H^{(n)}$ are excited with n diffractions from the second crystal (diffraction vector $\mathbf{H} + \Delta\mathbf{H}$) and with $n-1$ from the first crystal (diffraction vector $-\mathbf{H}$). The wave vectors $\mathbf{k}_0^{(n)}$ are due to n diffractions from the second crystal and to as many from the first crystal. All these wave vectors are vacuum wave vectors, $\mathbf{k}_G^{(n)} = \mathbf{k}_0 + \mathbf{G} + n\Delta\mathbf{H} - g_G^{(n)}\mathbf{n}$, where $g_0^{(n)} = n\Delta\mathbf{H} \cdot \mathbf{s}_0/\gamma_0$, $g_H^{(n)} = g_H + n\Delta\mathbf{H} \cdot \mathbf{s}_H/\gamma_H$, and $\mathbf{G}$ is either $\mathbf{0}$ or $\mathbf{H}$. The vector $\mathbf{k}_0^{(n)}$ excites the waves in the first and in the second crystal that are described by the matrices $\mathbf{A}^{(n)}$ and $\mathbf{B}^{(n)}$, respectively. Thus, the deviation parameters in the first crystal (index A) and the second crystal (index B) are found with equation (8) using $\mathbf{k}_0^{(n)}$ and the diffraction vector in the first ($\mathbf{H}$) and in the second crystal ($\mathbf{H} + \Delta\mathbf{H}$) instead of $\mathbf{k}_0$ and $\mathbf{H}$:

$$\begin{aligned} \eta_A^{(n)} &= \eta - n\Lambda_0 \Delta\mathbf{H} \cdot (\mathbf{s}_H/\gamma_H - \mathbf{s}_0/\gamma_0) \\ \eta_B^{(n)} &= \eta_A^{(n)} - \Lambda_0(\Delta\mathbf{H} \cdot \mathbf{s}_H)/\gamma_H. \end{aligned} \tag{12}$$

Now the elements in the matrix $\mathbf{A}^{(n)}$ are obtained from (10) with the following replacements: $\eta \rightarrow \eta_A^{(n)}$, $\mathbf{k}_0 \rightarrow \mathbf{k}_0^{(n)}$ and $\mathbf{k}_H \rightarrow \mathbf{k}_H^{(n)}$. The elements of the matrix $\mathbf{B}^{(n)}$ are obtained with the replacements: $\eta \rightarrow \eta_B^{(n)}$, $\mathbf{k}_0 \rightarrow \mathbf{k}_0^{(n)}$, $\mathbf{k}_H \rightarrow \mathbf{k}_H^{(n+1)}$, $t_A \rightarrow t_B$, $a \rightarrow a'$, $e \rightarrow e'$ and $\mathbf{H} \rightarrow \mathbf{H} + \Delta\mathbf{H}$. The coefficients for the transition through the gap are the same as given in Appendix *B*. The following matrix equations are read from Fig. 1:

$$\begin{bmatrix} e_{0,a}^{(0)} \\ 0 \end{bmatrix} = \mathbf{A}^{(0)} \begin{bmatrix} e_{0,e} \\ e_{H,e}^{(0)} \end{bmatrix}, \quad \begin{bmatrix} e_{0,a'}^{(0)} \\ 0 \end{bmatrix} = \mathbf{B}^{(n)} \begin{bmatrix} e_{0,a}^{(n)} \\ e_{H,a}^{(n+1)} \end{bmatrix},$$
$$n > 0: \quad \begin{bmatrix} e_{0,a}^{(n)} \\ e_{H,a}^{(n)} \end{bmatrix} = \mathbf{A}^{(n)} \begin{bmatrix} 0 \\ e_{H,e}^{(n)} \end{bmatrix}. \tag{13}$$

From these expressions, a recursion formula for the diffracted intensities is derived:

$$\begin{aligned} e_{H,e}^{(0)} &= -\frac{\rho_{HA}^{(0)}}{\tau_{HA}^{(0)}} \frac{\varphi_{0H,A}^{(0)}}{\varphi_{HH,A}^{(0)}} e_{0,e} \\ e_{H,e}^{(1)} &= -\frac{\Gamma_0}{\Gamma_H} \frac{\Psi_A^{(0)}}{\Psi_A^{(1)}} \frac{\rho_{HB}^{(0)}}{\tau_{HA}^{(0)} \tau_{HA}^{(1)} \tau_{HB}^{(0)}} \frac{\varphi_{0H,B}^{(0)}}{\varphi_{HH,B}^{(0)} \varphi_{HH,A}^{(1)}} e_{0,e} \\ e_{H,e}^{(n+1)} &= -\frac{\Gamma_0}{\Gamma_H} \frac{\Psi_A^{(n)}}{\Psi_A^{(n+1)}} \frac{\rho_{0A}^{(n)} \rho_{HB}^{(n)}}{\tau_{HA}^{(n+1)} \tau_{HB}^{(n)}} \frac{\varphi_{H0,A}^{(n)} \varphi_{0H,B}^{(n)}}{\varphi_{HH,A}^{(n+1)} \varphi_{HH,B}^{(n)}} e_{0,e}^{(n)}. \end{aligned} \tag{14}$$

From these equations, one obtains:

$$e_{H,e}^{(n>1)} = (-1)^n \left(\frac{\Gamma_0}{\Gamma_H}\right)^n \frac{\Psi_A^{(0)}}{\Psi_A^{(n)}} \frac{\rho_{HB}^{(0)}}{\tau_{HA}^{(0)}\tau_{HA}^{(1)}\tau_{HB}^{(0)}} \times \prod_{j=2}^{n}\left[\frac{\rho_{0A}^{(j-1)}\rho_{HB}^{(j-1)}}{\tau_{HA}^{(j)}\tau_{HB}^{(j-1)}}\right] \frac{\varphi_{0H,B}^{(0)}}{\varphi_{HH,B}^{(0)}\varphi_{HH,A}^{(1)}} \times \prod_{j=2}^{n}\left[\frac{\varphi_{H0,A}^{(j-1)}\varphi_{0H,B}^{(j-1)}}{\varphi_{HH,A}^{(j)}\varphi_{HH,B}^{(j-1)}}\right] e_{0,e}, \tag{15}$$

where

$$\frac{\varphi_{0H,A}^{(0)}}{\varphi_{HH,A}^{(0)}} = \exp[2\pi i g_H^{(0)}\mathbf{n}\cdot\mathbf{r}_e],$$

$$\frac{\varphi_{0H,B}^{(0)}}{\varphi_{HH,B}^{(0)}\varphi_{HH,A}^{(1)}} = \exp[2\pi i g_H^{(1)}\mathbf{n}\cdot\mathbf{r}_e]\exp[2\pi i g_0^{(1)}t_A] \times \exp[2\pi i g_H^{(1)}t_g], \tag{16}$$

$$\prod_{j=2}^{n}\left[\frac{\varphi_{H0,A}^{(j-1)}\varphi_{0H,B}^{(j-1)}}{\varphi_{HH,A}^{(j)}\varphi_{HH,B}^{(j-1)}}\right] = \exp\{2\pi i[g_0^{(n)} - g_0^{(1)}]t_A\} \times \exp\{2\pi i[g_H^{(n)} - g_H^{(1)}]\mathbf{n}\cdot\mathbf{r}_e\} \times \exp\left\{2\pi i\sum_{j=2}^{n}[g_H^{(j)} - g_0^{(j-1)}]t_g\right\}.$$

For a position $\mathbf{r}_S = \mathbf{r}_e + \mathbf{x}$ in the entrance surface ($\mathbf{x}\cdot\mathbf{n} = 0$) of the bicrystal, one then finds the expressions given in equations (5). These equations are very general and must be evaluated numerically in most cases. However, for special cases, analytical expressions can be found. Such cases will now be discussed.

*C*1. *Reciprocal-lattice vector difference perpendicular to the diffraction plane*

For a $\Delta\mathbf{H}$ perpendicular to the diffraction plane, $\Delta\mathbf{H}\cdot\mathbf{s}_0 = \Delta\mathbf{H}\cdot\mathbf{s}_H = 0$. Then it follows from equation (12) that $\eta_A^{(n)} = \eta_B^{(n)} = \eta$ for all diffraction orders. This means that the wavefields in both crystals are described with the same deviation parameter. Now, the phase $\Phi_{\text{Bragg}}^{(n)}$ in (5*b*) can be written as $\Phi_{\text{Bragg}}^{(n)} = n\Phi$, where Φ does not depend on n.

*C*2. *Reciprocal-lattice vector difference perpendicular to the sample surface*

For a $\Delta\mathbf{H}$ perpendicular to the sample surface, $\Delta\mathbf{H} = \Delta H\mathbf{n}$. Now, equation (12) shows that $\eta_A^{(n)} = \eta$ and $\eta_B^{(n)} = \eta - \Lambda_0\Delta\mathbf{H}\cdot\mathbf{s}_H/\gamma_H$. This means that the deviation parameters of all diffraction orders are the same in each of the crystal plates but they are different between the two crystals. This also allows one to write the phases $\Phi_{\text{Bragg}}^{(n)}$ in (5*b*) as $\Phi_{\text{Bragg}}^{(n)} = n\Phi$ with Φ again independent of n.

For both the above cases, the sum in (15) can now be evaluated by rewriting it in the form of a geometrical series $1 - x + x^2 - x^3 + \ldots = (1+x)^{-1}$:

$$\begin{aligned} I_H^{\text{tot}}(\mathbf{r}_s) &= \left|\frac{\rho_{HA}}{\tau_{HA}} + \exp(2\pi i\Phi)\frac{\rho_{HB}}{\tau_{HA}^2\tau_{HB}}\left\{1 + \sum_{n=2}^{\infty}(-1)^{n-1} \times \left[\exp(2\pi i\Phi)\frac{\rho_{HB}\rho_{0A}}{\tau_{HB}\tau_{HA}}\right]^{n-1}\right\}\right|^2 \\ &= \left|\frac{\rho_{HA}}{\tau_{HA}} + \exp(2\pi i\Phi)\frac{\rho_{HB}}{\tau_{HA}^2\tau_{HB}} \times \left[1 + \exp(2\pi i\Phi)\frac{\rho_{HB}\rho_{0A}}{\tau_{HB}\tau_{HA}}\right]^{-1}\right|^2 \\ &= \left|\frac{\rho_{HA}\tau_{HB} + \exp(2\pi i\Phi)\tau_{0A}\rho_{HB}}{\tau_{HA}\tau_{HB} + \exp(2\pi i\Phi)\rho_{0A}\rho_{HB}}\right|^2. \end{aligned} \tag{17}$$

This final expression can further be looked at for special cases. For a vanishing reciprocal-lattice vector difference, $\Delta\mathbf{H} = 0$, one obtains the gap and crystal thickness oscillations when a rocking curve is measured in the Bragg case. If in addition the gap thickness vanishes, $t_g = 0$, then $\Phi = 0$ and equation (17) leads to the expression for the intensity diffracted by a single crystal of thickness $t_A + t_B$.

APPENDIX *D*
Moiré fringes recorded with different topographic techniques in the Laue case

To simplify the expressions and also to evidence the fundamental effects, only the cases where $\Lambda_0\Delta\mathbf{H}\cdot\mathbf{s}_H/\gamma_H \ll 1$ and $\Lambda_0\Delta\mathbf{H}\cdot\mathbf{s}_0/\gamma_0 \ll 1$ are investigated. This leads to $\eta \approx \eta_0 \approx \eta_H$ [see equation (8)]. Furthermore, a negligible gap thickness ($\Phi_{\text{gap}} \simeq 0$) and zero absorption are considered. This means that the *Pendellösung* length Λ_0 and the normalized crystal thicknesses $A_A = \pi t_A/\Lambda_0$ and $A_B = \pi t_B/\Lambda_0$ are real quantities. Omitting the global factor $|(\gamma_0\chi_H/\gamma_H\chi_{\bar{H}})e_{0,e}|^2$, the diffracted intensity is then:

$$\begin{aligned} I_H(\mathbf{r}_S) &= \hat{I}_H + \Delta I_{H,c}\cos(2\pi\Phi_{\text{Laue}}) + \Delta I_{H,s}\sin(2\pi\Phi_{\text{Laue}}) \\ \hat{I}_H &= [\sin^2(A_A y) + \sin^2(A_B y)]/y^2 - 2[\sin^2(A_A y)\sin^2(A_B y)]/y^4 \\ \Delta I_{H,c} &= [\sin(2A_A y)\sin(2A_B y)]/2y^2 - 2\eta^2[\sin^2(A_A y)\sin^2(A_B y)]/y^4 \\ \Delta I_{H,s} &= (2\eta/y^3)\sin[(A_A + A_B)y]\sin(A_A y) \times \sin(A_B y). \end{aligned} \tag{18}$$

Expressions (18) can be used to investigate the properties of moiré fringes under several experimental condi-

tions: a very small η range, $\Delta\eta$, used to record the topograph corresponds to highly collimated and highly monochromatic radiation. For a larger $\Delta\eta$, equations (18) must be integrated.

To perform such an integration, approximations can be made for the functions that appear in (18). Therefore, the function $\sin(Ay)$ with A as an arbitrary constant and $y = (1+\eta^2)^{1/2}$ needs to be discussed. This function first equals zero for values of η that are closer to $\eta = 0$ than $\pm\pi/A$; beyond these positions, $\sin(Ay)$ has an oscillatory character and $\sin(Ay) \approx \sin(A|\eta|)$ for $\eta \gg 1$. Thus, when $A \gg 1$ and an integral of a product of $[\sin(Ay)]^n$ and an arbitrary but slowly varying $f(\eta)$ is to be found, $[\sin(Ay)]^n$ can be approximated by $[\sin(A|\eta|)]^n$ because the error made in this way (mainly in the range $-\pi/A < \eta < \pi/A$) can be neglected. For a range of integration $\Delta\eta \gg \pi/A$, this leads to the following approximations:

$$\begin{aligned}
&\int f(\eta)\sin(Ay)\,\mathrm{d}\eta \approx 0\\
&\int f(\eta)\sin^2(Ay)\,\mathrm{d}\eta \approx (A/2\pi)\int_0^{2\pi/A}\sin^2(A\eta)\,\mathrm{d}\eta \int f(\eta)\,\mathrm{d}\eta\\
&\qquad = \tfrac{1}{2}\int f(\eta)\,\mathrm{d}\eta\\
&\int f(\eta)\sin^4(Ay)\,\mathrm{d}\eta \approx (A/2\pi)\int_0^{2\pi/A}\sin^4(A\eta)\,\mathrm{d}\eta \int f(\eta)\,\mathrm{d}\eta\\
&\qquad = \tfrac{3}{8}\int f(\eta)\,\mathrm{d}\eta. \qquad (19)
\end{aligned}$$

*D*1. *Radiation of high collimation and monochromaticity*

This situation appears when $\Delta\eta \ll \Lambda_0/(t_A + t_B)$ and thus equations (18) need not be integrated. The moiré pattern is then given by a cosine and a sine term multiplied by factors that depend on the deviation parameter, as does the position of the moiré pattern itself. Expressions (18) can then be transformed into

$$I_H(\mathbf{r}_S) = \hat{I}_H + \Delta I_H \cos[2\pi(\Delta\mathbf{H}\cdot\mathbf{r}_S + \Phi_{\Delta\mathbf{H},\mathrm{Laue}} - \varphi)]$$

using the relation

$$a\cos x + b\sin x = (a^2+b^2)^{1/2}\cos[x - \arctan(b/a)],$$

where

$$\begin{aligned}
2\pi\varphi = \arctan\big((\eta/y)\sin[(A_A + A_B)y]\\
\times\{\cos(A_A y)\cos(A_B y)\\
-(\eta^2/y^2)[\sin(A_A y)\sin(A_B y)]\}^{-1}\big). \qquad (20)
\end{aligned}$$

For the case of electron diffraction, such an equation is called a 'displacement equation' of the moiré fringe pattern (Gevers, 1962; Allinson, 1968). Equations (19) show that, for $|\eta| \gg 1$, the displacement equation is $2\pi\varphi \simeq \eta(A_A + A_B)$. Hence, on plane monochromatic wave topographs, the moiré pattern is translated over one fringe spacing when the deviation parameter is varied by $\Delta\eta = \Delta\Theta/\omega_0 = 2\Lambda_0/(t_A + t_B)$.

*D*2. *Radiation of medium collimation and monochromaticity*

This situation arises when $\Lambda_0/(t_A + t_B) \ll \Delta\eta \ll 1$ and is typical for many topographical experiments. Expressions (18) must then be integrated over the range $\Delta\eta$. This is performed by using the approximations (19). Within this range, the sine functions in (18) may have several oscillations. In the present context concerning the displacement of the moiré pattern with a variation of the deviation parameter, only the functions $\Delta I_{H,s}$ and $\Delta I_{H,c}$ are of interest. The results are denoted $\Delta I_{H,s}^{(\Delta\eta)}$ and $\Delta I_{H,c}^{(\Delta\eta)}$ to indicate the range of the integration.

When $t_A \gg \Lambda_0$ and $t_B \gg \Lambda_0$, then $\Delta I_{H,s}^{(\Delta\eta)} \approx 0$ and, consequently, the position of the moiré pattern does not depend on the deviation parameter. However, for $t_A \gg \Lambda_0$ and $t_B \ll \Lambda_0$, the functions $\Delta I_{H,s}^{(\Delta\eta)} \approx \Delta\eta(\eta^2)\times \sin^2(A_B y)/y^4$ and $\Delta I_{H,c}^{(\Delta\eta)} \approx (1/2)\Delta\eta(\eta)\sin(2A_B y)/y^3$, and the displacement equation is now $2\pi\varphi = -\arctan[y^*\cot(A_B y)/\eta]$. For the small values of A_B studied here, one finds, within a good approximation, that $2\pi\varphi \approx \eta^* A_B$ plus a constant phase shift. This means that, for the present case, a variation of $\Delta\Theta$ only results in a shift of a fraction $\Delta\Theta t_B/(2\omega_0\Lambda_0)$ of one moiré fringe spacing.

Thus, when both crystal plates are much thicker than the *Pendellösung* length, no displacement of the moiré fringe pattern with a deviation η from the exact Bragg position is expected. When one plate is much thicker and the other much thinner than the *Pendellösung* length, this displacement is, within a good approximation, a linear function in η, but the dependency is very weak.

*D*3. *Integrated wave topographs*

An 'integrated wave topograph' is recorded with $\Delta\eta \gg 1$ and expressions (18) can then be integrated over the deviation parameter from minus to plus infinity. Again, approximations (19) will be used for this purpose. The results will then be denoted $\hat{I}_H^{(\infty)}$, $\Delta I_{H,c}^{(\infty)}$ and $\Delta I_{H,s}^{(\infty)}$. Because $\Delta I_{H,s}$ in equations (18) is an odd function in η, $\Delta I_{H,s}^{(\infty)} \approx 0$. It is also seen that the integral over the forward-diffracted intensity diverges, which is expected for physical reasons. The function $\hat{I}_H^{(\infty)}$ is the sum of the integrated reflectivities of the two crystal plates and of an interference term. The moiré contrast $C^{\mathrm{moiré}} = |I_{\max} - I_{\min}|/(I_{\max} + I_{\min})$ is given by $\Delta I_{H,c}^{(\infty)}/\hat{I}_H^{(\infty)}$.

When $t_A \gg \Lambda_0$, $t_B \gg \Lambda_0$ and t_A and t_B are very different, the approximations (19) can be applied successively for the oscillating functions in equations (18). One obtains $\hat{I}_H^{(\infty)} \approx 3\pi/4$ and $\Delta I_{H,c}^{(\infty)} \approx -\pi/4$ and thus a moiré contrast of $C^{\mathrm{moiré}} = 1/3$. For $t_A \gg \Lambda_0$ and $t_A \approx t_B$, one obtains $\hat{I}_H^{(\infty)} \approx 5\pi/8$ and $\Delta I_{H,c}^{(\infty)} \approx -\pi/8$ and thus $C^{\mathrm{moiré}} = 1/5$ in this case. In other cases, when the approximations (19) cannot be applied, the integrations

need to be performed numerically. The moiré contrast then strongly depends on the *Pendellösung* length (see Fig. 2).

Claudio Ferrero (ESRF, Grenoble) is gratefully acknowledged for his assistance in finding and implementing a suitable numerical integration routine. The authors also wish to thank Rolf Köhler (Humboldt University, Berlin) and José Baruchel (ESRF, Grenoble) for fruitful discussions and reading the manuscript. We specially acknowledge the hints and suggestions given by Jun-ichi Yoshimura (Yamanashi University, Kofu). The referee reports led to significant improvements of the present paper.

References

Aboyan, A. O. & Arshakyan, E. Z. (1993). *Phys. Status Solidi A*, **137**, 57–66.
Allinson, D. L. (1968). *Philos. Mag.* **17**, 339–352.
Authier, A. (1961). *Bull. Soc. Fr. Minéral. Cristallogr.* **84**, 51–89.
Authier, A. (1967). *Adv. X-ray Anal.* **10**, 9–31.
Authier, A. (1992). *International Tables for X-ray Crystallography*, Vol. C, edited by A. J. C. Wilson, p. 464. Dordrecht: Kluwer.
Bassett, G. A., Menter, J. W. & Pashley, D. W. (1958). *Proc. R. Soc. London Ser. A*, **246**, 345–368.
Batterman, B. W. & Cole, H. (1964). *Rev. Modern Phys.* **36**, 681–717.
Berreman, D. W. (1976). *Phys. Rev. B*, **14**, 4313–4317.
Bonse, U. & Hart, M. (1965). *Appl. Phys. Lett.* **6**, 155–156.
Bonse, U. & Hart, M. (1968). *Phys. Status Solidi*, **33**, 351–359.
Bonse, U., Hart, M. & Schwuttke, G. H. (1969). *Phys. Status Solidi*, **33**, 361–374.
Chikawa, J. (1965). *Appl. Phys. Lett.* **7**, 193–195.
Chikawa, J. (1967). *J. Phys. Chem. Solids*, **28**(Suppl. 1), 817–823.
Gaca, J. (1974). *Phys. Status Solidi A*, **26**, 305–310.
Gerward, L. (1978). *Philos. Mag.* A**37**, 95–106.
Gevers, R. (1962). *Philos. Mag.* **7**, 1681–1720.
Hart, M. (1975). *Proc. R. Soc. London Ser. A*, **346**, 1–22.
Härtwig, J., Holý, V., Kittner, R., Kubena, J. & Lerche, V. (1988). *Phys. Status Solidi A*, **104**, 61–75.
Hashimoto, H., Mannami, M. & Naiki, T. (1961). *Philos. Trans. R. Soc. London*, **253**, 490–516.
Jiang, B. L., Shimura, F. & Rozgonyi, G. A. (1990). *Appl. Phys. Lett.* **56**, 352–354.
Kato, N. (1974). *X-ray Diffraction*, edited by L. V. Azaroff, R. Kaplow, N. Kato, R. J. Weiss, A. J. C. Wislon & R. A. Young, pp. 380–389. New York: McGraw-Hill.
Kuběna, J. & Holý, V. (1983). *Czech. J. Phys.* B**33**, 1315–1322.
Lang, A. R. (1968). *Nature (London)*, **220**, 652–657.
Laue, M. (1960). *Röntgenstrahlinterferenzen*. Frankfurt am Main: Akademische Verlagsanstalt.
Mitsuishi, T., Nagasaki, H. & Uyda, R. (1951). *Proc. Jpn. Acad.* **27**, 86–87.
Ohler, M., Härtwig, J. & Prieur, E. (1997). *Acta Cryst.* A**53**, 199–201.
Ohler, M., Köhler, S. & Härtwig, J. (1999). *Acta Cryst.* A**55**, 423–432.
Ohler, M., Prieur, E. & Härtwig, J. (1996). *J. Appl. Cryst.* **29**, 568–573.
Polcarová, M. (1978). *Phys. Status Solidi A*, **46**, 567–575; **47**, 179–186.
Polcarová, M. (1980). *Phys. Status Solidi A*, **59**, 779–785.
Prieur, E., Ohler, M. & Härtwig, J. (1996). *Phys. Status Solidi A*, **158**, 19–34.
Simon, D. & Authier, A. (1968). *Acta Cryst.* A**24**, 527–534.
Tanner, B. K. (1996). *X-ray and Neutron Dynamical Diffraction, Theory and Applications*, *NATO ASI Series, Series B, Physics*, Vol. 357, edited by A. Authier, S. Lagomarsino & B. K. Tanner, p. 149. New York: Plenum.
Yoshimura, J. (1991). *Phys. Status Solidi A*, **125**, 429–440.
Yoshimura, J. (1996). *Acta Cryst.* A**52**, 312–325.
Zachariasen, W. H. (1945). *Theory of X-ray Diffraction in Crystals*. New York: John Wiley.